

Molecular Physics

An International Journal at the Interface Between Chemistry and Physics

ISSN: 0026-8976 (Print) 1362-3028 (Online) Journal homepage: <http://www.tandfonline.com/loi/tmph20>


Damping functions in the effective fragment potential method

Lyudmila V. Slipchenko & Mark S. Gordon


To cite this article: Lyudmila V. Slipchenko & Mark S. Gordon (2009) Damping functions in the effective fragment potential method, *Molecular Physics*, 107:8-12, 999-1016, DOI: [10.1080/00268970802712449](https://doi.org/10.1080/00268970802712449)



To link to this article: <http://dx.doi.org/10.1080/00268970802712449>

 View supplementary material 

 Published online: 07 Oct 2010.

 Submit your article to this journal 

 Article views: 294

 View related articles 

 Citing articles: 50 View citing articles 

INVITED ARTICLE

Damping functions in the effective fragment potential method

Lyudmila V. Slipchenko† and Mark S. Gordon*

Department of Chemistry and Ames Laboratory, Iowa State University,
Ames, IA 50011, USA

(Received 3 December 2008; final version received 19 December 2008)

This work presents the implementation and analysis of several damping functions for Coulomb, induction, and dispersion interactions within the framework of the general effective fragment potential (EFP) method. Damping is necessary to obtain the correct asymptotic short-range behavior of these interactions. Correctly chosen damping functions allow a balanced description of different parts of intermolecular potential energy surfaces and improve the accuracy of predicted intermolecular distances and binding energies. The performance of different damping functions is tested by comparing the EFP energy terms with the symmetry adapted perturbation theory (SAPT) energy terms in a range of intermolecular separations for ten molecular dimers. The total EFP binding energies in these dimers were compared with the binding energies obtained from SAPT and coupled cluster theory with single, double, and perturbative triple excitations [CCSD(T)]. A formula for electrostatic damping that was derived from first principles is recommended. This method employs the overlap of fragment localized molecular orbitals (LMO) within the spherical Gaussian approximation. The LMO overlap integrals are also used to determine the damping of dispersion. Gaussian polarization damping functions are recommended for use within the EFP framework. With this set of damping functions, the EFP binding energies are within 0.5 kcal/mol and intermolecular equilibrium separations are within 0.2 Å of the corresponding CCSD(T) and SAPT values. This consistent accuracy of EFP is encouraging for future studies of more complicated molecular complexes.

Keywords: intermolecular interactions; force field; effective fragment potential method; screening; damping functions; Coulomb interactions; polarization; dispersion

1. Introduction

Modelling intermolecular interactions plays an important role in studying liquids, molecular clusters, surface catalysis, and bio-systems; therefore, it is of interest in many fields of chemistry, physics, biological sciences and materials. However, accurate representation of intermolecular interactions is a non-trivial task for quantum chemistry. High-level *ab initio* calculations can adequately describe weak intermolecular forces in systems of small size. However, the accuracy of *ab initio* calculations depends on both the basis set size and the amount of dynamic correlation that is included in the calculation. As a result, calculations of sufficient accuracy are very computationally demanding and rapidly become impractical as the system size increases.

Alternatively, one can describe intermolecular interactions using perturbation theory, starting from the non-interacting (unperturbed) fragments. In the last decade, this idea has been developed within the context of the general effective fragment potential (EFP) method [1–3]. In terms of perturbation theory,

intermolecular interactions can be presented as a series of short- and long-range terms. Long-range interactions, which are proportional to the distance according to $(1/R)^n$, include Coulomb, induction, and dispersion terms, whereas short-range interactions, which decay exponentially, consist of exchange-repulsion, charge-transfer, and screening terms. Screening terms are used to ensure that the contributions derived from the long-range perturbation theory, i.e. induction, dispersion, and Coulomb, do not diverge when molecules approach each other. It has been shown that inclusion of screening terms is crucial for accurate modelling of many systems ranging from hydrogen-bonded water to the benzene dimer [4,5]. Moreover, a physically correct shape of the potential at short distances is essential for an accurate description of dynamic properties of clusters and liquids, as well as of more strongly interacting species such as charged molecules and ions. The decrease in accuracy of the perturbative approach at short distances, in regions where screening becomes important, signals an increase in strong interactions, such as incipient ionic or

*Corresponding author. Email: mark@si.msg.chem.iastate.edu

†Current address: Department of Chemistry, Purdue University, West Lafayette, IN 47907.

covalent bonding. For this reason the development of a physically meaningful and computationally inexpensive formulation of screening terms is not trivial. In the current implementation of the EFP method, dispersion interaction energies are screened using the Tang–Toennies damping formulas [6,7]. Screening of Coulomb terms is accomplished using elaborate exponential expressions with parameters derived from matching the electrostatic multipole potential of a molecule with its *ab initio* potential [4,5]. Induction interactions have so far been treated without any screening.

The present work investigates the accuracy of screening terms for the Coulomb and dispersion interaction energies in the EFP method. Additionally, various approaches to the damping of induction (polarization) energies are derived and implemented. The accuracy of the screened EFP electrostatic, induction, and dispersion terms is analyzed for ten molecular dimers, by comparing the EFP energies with the symmetry adapted perturbation theory [8] (SAPT) energies. Based on this extensive analysis, recommendations are given on an optimal choice of screening procedures in the EFP method.

The structure of the paper is as follows: The next section gives a theoretical description of the EFP method; Section 3 provides computational details. Sections 4 to 6 discuss damping schemes in the electrostatic, dispersion, and polarization terms, respectively. The analysis of the total interaction energies is presented in Section 7; while our final conclusions are given in Section 8.

2. EFP theory

All of the terms in the EFP method may be thought of as truncated expansions. At present, the EFP interaction energy is a sum of five terms [2]:

$$E = E_{coul} + E_{ind} + E_{exrep} + E_{disp} + E_{ct} \quad (1)$$

Equation (1) specifically refers to EFP–EFP interactions. E_{coul} refers to the Coulomb portion of the electrostatic interaction. This term is obtained using the distributed multipolar expansion introduced by Stone [9], with the expansion carried out through octopoles. E_{ind} is the induction or polarization part of the electrostatic interaction. This term is represented by the interaction of the induced dipole on one fragment with the electrostatic field on another fragment, expressed in terms of the dipole polarizability. The molecular polarizability is expressed as a tensor sum of localized molecular orbital (LMO) polarizabilities. That is, the number of polarizability points is equal to

the number of bonds and lone pairs in the molecule. These induced dipoles are iterated to self-consistency, so some many body effects are included.

The exchange repulsion E_{exrep} is derived as an expansion in the intermolecular overlap, truncated at the quadratic term [10]. This term does require that each EFP carries a basis set, and the smallest recommended basis set is 6-31++G(d,p) [11] for acceptable results. Since the basis set is used only to calculate overlap integrals, the computation is very fast and quite large basis sets are realistic. The dispersion interaction can be expressed as the familiar inverse R expansion,

$$E_{disp} = \sum_n C_n R^{-n}. \quad (2)$$

The coefficients C_n may be derived from the (imaginary) frequency dependent polarizabilities summed over the entire frequency range [6,12]. If one employs only dipole polarizabilities the dispersion expansion is truncated at the leading term, with $n=6$. In the current EFP code, an estimate is used for the $n=8$ term, in addition to the explicitly derived $n=6$ term. Rather than express a molecular C_6 as a sum over atomic interaction terms, the EFP dispersion is expressed in terms of LMO–LMO interactions.

The charge transfer interaction E_{ct} is derived by considering, using a supermolecule approach, the interactions between the occupied valence molecular orbitals on one fragment with the virtual orbitals on another fragment. This leads to significant energy lowering in *ab initio* calculations on ionic or highly polar species when incomplete basis sets are employed. An approximate formula [13] for the charge transfer interaction in the EFP method was derived and implemented using a second order perturbative treatment of the intermolecular interactions for a pair of molecules at the Hartree–Fock level of theory. The approximate formula is expressed in terms of canonical orbitals from Hartree–Fock calculations of independent molecules and uses a multipolar expansion (through quadrupoles) of the molecular electrostatic potentials.

In its present implementation, EFP does not include any cross-terms which appear when the intermolecular interaction energy is expanded in polarization and in exchange series. For example, symmetry adapted perturbation theory includes exchange-induction and exchange-dispersion terms [8] that are not currently included in the EFP formulation. The exchange-induction term is thought to be similar in value but opposite in sign to the charge-transfer term [14]. The exchange-dispersion interaction usually does not exceed ~ 15 – 25% of the dispersion energy and somewhat cancels higher-order terms (R^{-8} , R^{-10} , etc.)

of the dispersion expansion. Thus, the success of the EFP method may depend on a favourable cancellation of the exchange-induction and charge-transfer terms, and the exchange-dispersion and higher-order dispersion terms. From this point of view, it is not necessary to include the charge-transfer term in EFP. Indeed, this approach has been used for modeling non-charged species with EFP [15–17].

3. Computational details

All calculations were performed with the quantum chemistry program GAMESS [18,19].

Equilibrium geometries of the methane, H₂, methanol, and ammonia dimers were adapted from [6]; the CH₂Cl₂ dimer geometry is from [5]. The geometry of the HF dimer is the geometry from [20], obtained at the coupled cluster with single, double, and perturbative triple excitations [21] [CCSD(T)] in the complete basis set limit (CBS); the Ar dimer geometry is the CCSD(T)/aug-cc-pVQZ [22,23] geometry from [24]. The water monomer was optimized at the CCSD(T)/cc-pVTZ level of theory [22], then the geometry of the dimer was obtained by a constrained optimization at the MP2²⁵/6-311++G(3df, 2p) [26–28] level of theory. The benzene dimer geometries are from [29]. These geometries can be viewed in the Supplementary Materials section.

For all dimers except the benzene dimer, the separation between the monomers was varied in the range from –0.8 to +0.8 Å with increments of 0.2 Å with respect to their equilibrium geometries. For benzene, two configurations were considered, the sandwich structure and the T-shaped structure. The separation between benzene rings was varied from 3.3 Å to 6.0 Å in the sandwich and from 4.7 Å to 6.9 Å in the T-shaped structure. SAPT and CCSD(T) data are used to benchmark the EFP results. The 6-311++G(3df, 2p) basis set is used to generate the EFP for Ar, H₂, water, methane, ammonia, and HF, and in the SAPT and CCSD(T) calculations on the respective dimers; the 6-311++G(2d, 2p) basis [26–28] is employed for the methanol dimer; the 6-31+G* basis [26,30,31] is used for the CH₂Cl₂ dimer. The 6-311++G(3df, 2p) basis is used for EFP calculations on benzene dimer. The SAPT and CCSD(T) data are from [32], they were obtained in the aug-cc-pVDZ basis and estimated in the aug-cc-pVQZ bases, respectively.

4. Damping of the electrostatic energy

The Coulomb intermolecular forces in EFP are modeled by classical interactions of distributed

multipoles centred at each atom and bond mid-point. So, for water, there are five expansion points (three at the atom centres and two at the O–H bond midpoints), while in benzene there are 24 expansion points. Multipoles for each fragment are obtained from the distributed multipolar analysis (DMA) originated by Stone [9]. In this approach, the Coulomb potential is expanded in a series of terms in (1/R):

$$V = Tq - T_{\alpha}\hat{\mu}_{\alpha} + \frac{1}{3}T_{\alpha\beta}\hat{\Theta}_{\alpha\beta} - \frac{1}{15}T_{\alpha\beta\gamma}\hat{\Omega}_{\alpha\beta\gamma} + \dots, \quad (3)$$

where T are the electrostatic tensors of 0, 1, 2, etc. ranks, and q , μ_{α} , $\Theta_{\alpha\beta}$, $\Omega_{\alpha\beta\gamma}$ are the point charge, dipole, quadrupole, and octopole. The formulas for T are given in Appendix A. In the EFP method, the Coulomb potential is expanded up to octopoles [1]. The Coulomb energy of two interacting molecules (A and B) can be evaluated according to the formulas for classical multipolar interactions:

$$\begin{aligned} E^{AB} &= q^B \left[Tq^A - T_{\alpha}\hat{\mu}_{\alpha}^A + \frac{1}{3}T_{\alpha\beta}\hat{\Theta}_{\alpha\beta}^A - \frac{1}{15}T_{\alpha\beta\gamma}\hat{\Omega}_{\alpha\beta\gamma}^A + \dots \right] \\ &\quad + \hat{\mu}_{\alpha}^B \left[T_{\alpha}q^A - T_{\alpha\beta}\hat{\mu}_{\beta}^A + \frac{1}{3}T_{\alpha\beta\gamma}\hat{\Theta}_{\beta\gamma}^A - \dots \right] \\ &\quad + \hat{\Theta}_{\alpha\beta}^B \left[T_{\alpha\beta}q^A - T_{\alpha\beta\gamma}\hat{\mu}_{\gamma}^A + \frac{1}{3}T_{\alpha\beta\gamma\delta}\hat{\Theta}_{\gamma\delta}^A - \dots \right] \\ &\quad + \hat{\Omega}_{\alpha\beta\gamma}^B \left[-\frac{1}{15}T_{\alpha\beta\gamma}q^A + \dots \right] \\ &= Tq^A q^B + T_{\alpha}(q^A \hat{\mu}_{\alpha}^B - \hat{\mu}_{\alpha}^A q^B) \\ &\quad + T_{\alpha\beta} \left(\frac{1}{3}q^A \hat{\Theta}_{\alpha\beta}^B + \frac{1}{3}\hat{\Theta}_{\alpha\beta}^A q^B - \hat{\mu}_{\alpha}^A \hat{\mu}_{\beta}^B \right) + \dots, \quad (4) \end{aligned}$$

where q^A is the charge on centre A, q^B is the charge on centre B, etc.

The Coulomb point multipole model breaks down if fragments approach each other too closely, because then the actual electron densities on the fragments are not well approximated by point multipoles. The electrostatic interactions become too repulsive and must be moderated by a screening or damping term [4,5]. Several approaches for damping classical Coulomb energies have been discussed in the literature. Two of these approaches are summarized here, i.e. (1) damping with exponential functions using the parameters derived from matching the classical electrostatic potential with the *ab initio* potential [5]; and (2) damping using the orbital overlap formula derived by Kairys and Jensen [33].

4.1. Exponential damping

Various damping functions and their derivation were discussed in detail in [5], so only a brief summary is

presented here. The following form is assumed for the damped charge potential:

$$V^{ch} = Tq(1 + f_0) \quad (5)$$

where f_0 is the damping function, taken here to be [5]:

$$f_0 = -\exp(-\alpha R) \quad (6)$$

where α is the damping parameter. The damped potentials of dipole and higher multipoles can be evaluated by expanding the damped charge potential as a Taylor series, similar to the procedure for obtaining classical multipole potentials. This results in:

$$\begin{aligned} V^{dip} &= T_\alpha \hat{\mu}_\alpha (1 + f_1) \\ V^{quad} &= \frac{1}{3} \hat{\Theta}_{\alpha\beta} [T_{\alpha\beta} (1 + f_1) + D_{\alpha\beta} f_2]. \end{aligned} \quad (7)$$

The additional tensors $D_{\alpha\beta}$ and damping functions f_1 and f_2 are given in Appendix A. The damping parameters α appearing in the damping functions are different for each expansion centre; they are determined by fitting the damped multipole potential to the quantum mechanical potential on the grid of points surrounding the EFP fragment.

Using the new damped electrostatic potential, one can derive the expressions for damped electrostatic energies. By introducing a new set of damping functions P , which are related to the functions f , the different parts of the electrostatic energy can be written as follows:

$$E_{AB}^{ch-ch} = T \left[q_e^B q_e^A (1 + P_0(\alpha, \beta)) + q_e^B Z^A (1 + P_0(\infty, \beta)) \right. \\ \left. + q_e^A Z^B (1 + P_0(\alpha, \infty)) + Z^B Z^A \right] \quad (8a)$$

$$\begin{aligned} E_{AB}^{ch-dip} &= T_\alpha \hat{\mu}_\alpha^B [q_e^A (1 + P_1(\alpha, \beta)) + Z^A (1 + P_1(\infty, \beta))] \\ &\quad - T_\alpha \hat{\mu}_\alpha^A [q_e^B (1 + P_1(\alpha, \beta)) + Z^B (1 + P_1(\alpha, \infty))] \end{aligned} \quad (8b)$$

$$\begin{aligned} E_{AB}^{dip-dip} &= (\mu_\alpha^A \mu_\beta^B - \mu_\alpha^B \mu_\beta^A) \\ &\quad \times (\hat{T}_{\alpha\beta} (1 + P_1(\alpha, \beta)) + \hat{D}_{\alpha\beta} P_2(\alpha, \beta)) \end{aligned} \quad (8c)$$

$$\begin{aligned} E_{AB}^{ch-quad} &= \frac{1}{3} T_{\alpha\beta} \left[(\hat{\Theta}_{\alpha\beta}^A q_e^B + \hat{\Theta}_{\alpha\beta}^B q_e^A) (1 + P_1(\alpha, \beta)) \right. \\ &\quad \left. + \hat{\Theta}_{\alpha\beta}^B Z^A (1 + P_1(\infty, \beta)) + \hat{\Theta}_{\alpha\beta}^A Z^B \right. \\ &\quad \left. (1 + P_1(\alpha, \infty)) \right] \\ &\quad + \frac{1}{3} D_{\alpha\beta} \left[(\hat{\Theta}_{\alpha\beta}^A q_e^B + \hat{\Theta}_{\alpha\beta}^B q_e^A) P_2(\alpha, \beta) \right. \\ &\quad \left. + \hat{\Theta}_{\alpha\beta}^B Z^A P_2(\infty, \beta) + \hat{\Theta}_{\alpha\beta}^A Z^B P_2(\alpha, \infty) \right] \end{aligned} \quad (8d)$$

$$\begin{aligned} E_{AB}^{dip-quad} &= \frac{1}{3} (\hat{\mu}_\alpha^A \hat{\Omega}_{\beta\gamma}^B - \hat{\mu}_\alpha^B \hat{\Omega}_{\beta\gamma}^A) \\ &\quad \times \left[T_{\alpha\beta\gamma} (1 + P_1(\alpha, \beta)) \right. \\ &\quad \left. + P_4(\alpha, \beta) R_\alpha T_{\beta\gamma} + P_3(\alpha, \beta) R_\alpha D_{\beta\gamma} \right] \\ &\quad + \frac{2}{3} P_2(\alpha, \beta) (\hat{\mu}_\alpha^A R_\beta \hat{\Omega}_{\alpha\beta}^B - \hat{\mu}_\alpha^B R_\beta \hat{\Omega}_{\alpha\beta}^A) \end{aligned} \quad (8e)$$

where Z^A is the nuclear charge on atom A and ch =charge, dip =dipole, and $quad$ =quadrupole.

The energy damping functions $P_n(\alpha, \beta)$ for each pair of multipole expansion centres depend on two damping parameters, α and β , for centres A and B , respectively. These are the parameters that define damping in the electrostatic potential (see Equations (5)–(7)). The explicit formulas for the damping function are given in Appendix B.

All of the $P_n(\alpha, \beta)$ functions are symmetric with respect to the interchange of α and β . The exponential form of the damping functions suggests that they reach their maximum absolute values when the parameters approach 0, and become negligible when the parameters go to infinity. In other words, if any of the parameters α or β goes to infinity, there is no effective screening for this centre, as is the case for atomic nuclei.

The limiting values of $P(\alpha, \beta)$ when $\alpha = \beta$ and when the distance between centres approaches zero, $R \rightarrow 0$, are also given in Appendix B. Analysis of the energy expressions (Equations (8a)–(8e)) in the limit of $R \rightarrow 0$ shows that the damped charge–charge and charge–dipole energies become finite at $R \rightarrow 0$, with any values of α and β , whereas the dipole–dipole energy becomes finite only when $\alpha = \beta$ (note the tensor R -dependence $T \propto 1/R$, $T_\alpha \propto 1/R^2$, $T_{\alpha\beta} \propto 1/R^3$, etc.). Due to the presence of the $P(\infty, \beta)$ and $P(\alpha, \infty)$ terms, the charge–quadrupole energy becomes infinite ($1/R$) at small R . The damping functions do not completely eliminate the $R = 0$ singularity in the dipole–quadrupole energy, but this is a region that is unlikely to be sampled.

Damping only the charge–charge electrostatic energies captures the majority of the charge–penetration effect and does not require elaborate code development. Thus, we consider two models: one with charge–charge damping only, and the other one with the higher-order damping as well, i.e. with charge–charge, charge–dipole, charge–quadrupole, dipole–dipole, and dipole–quadrupole Coulomb terms damped.

4.2. Overlap formula for electrostatic damping

An alternative way to account for non-classical effects in the Coulomb energy was suggested by Kairys and

Jensen [33]. In this approach, the quantum (damping) corrections to the classical electrostatic energy are derived from the quantum-mechanical formulation of the electron interaction energy. If atomic orbitals are approximated by spherical Gaussians, the electron repulsion energy may be expressed as:

$$E_{e-e} = 4 \langle \chi_i \chi_i | \chi_j \chi_j \rangle = \frac{4}{R_{ij}} \text{erf}(\alpha R_{ij}), \quad (9)$$

where R_{ij} is the distance between the centres of the spherical Gaussians χ_i and χ_j :

$$\begin{aligned} \chi_i(r) &= \left(\frac{2\alpha}{\pi} \right)^{3/4} \exp(-\alpha |r - R_i|^2) \\ \chi_j(r) &= \left(\frac{2\alpha}{\pi} \right)^{3/4} \exp(-\alpha |r - R_j|^2). \end{aligned} \quad (10)$$

Expanding the error function in a series around the argument (αR_{ij}) and truncating after the second term, one can rewrite Equation (9) as:

$$\begin{aligned} E_{e-e} &= \frac{4}{R_{ij}} \text{erf}(\alpha R_{ij}) \approx \frac{4}{R_{ij}} \left(1 - \frac{1}{2\sqrt{\alpha} R_{ij}} \exp(-\alpha R_{ij}^2) \right) \\ &= \frac{4}{R_{ij}} - \frac{2}{\sqrt{\alpha} R_{ij}^2} \exp(-\alpha R_{ij}^2) = E_{e-e}^{\text{class}} + E_{e-e}^{\text{pen}}. \end{aligned} \quad (11)$$

Using the spherical Gaussian orbital (SGO) approximation [34], the penetration energy E^{pen} can be further simplified as:

$$E_{e-e}^{\text{pen}} = -2 \left(\frac{1}{-2 \ln |S_{ij}|} \right)^{1/2} \frac{S_{ij}^2}{R_{ij}}. \quad (12)$$

The latter equation uses the overlap integral S between the orbitals of the fragments and is similar to the SGO term in the exchange-repulsion energy in EFP [10]. The computation of Equation (12) does not involve significant additional cost. The penetration energy for each pair of fragments is calculated as a sum over contributions from the occupied molecular orbitals on each fragment.

4.3. Computational results

Figure 1 presents electrostatic energies in a set of weakly-bound dimers (Ar, H₂, methane, dichloromethane, ammonia, methanol, water, HF, and benzene dimers) calculated with different damping options. The EFP electrostatic energies without electrostatic screening (black curve), with exponential charge-charge and charge-charge + higher-order screening (blue and green curves, respectively), and with overlap-based screening (orange curve) are compared with the SAPT electrostatic energies (red curve). Since the

EFP electrostatic energy does not include any correlation, we compare the EFP energies with the HF part of the SAPT electrostatic energy. Correlation adds only a minor correction to the electrostatic energies in SAPT (usually within 2–5%).

For the hydrogen-bonded dimers of ammonia, water, HF, and methanol at their equilibrium distances (as defined in Section 3), the disagreement between the undamped (i.e. purely classical) EFP and SAPT Coulomb interaction energies is in the range of 0.8–1.2 kcal/mol (see Figure 1). The disagreement in the dispersion-bound complexes is in the range 0.02–2.2 kcal/mol. In the benzene dimer sandwich structure and in the methane dimer, the classical electrostatic energy (excluding damping) has the wrong sign: it is repulsive while the SAPT electrostatic energy is attractive. The discrepancy between the classical and quantum Coulomb interaction energies is due to quantum effects and is usually referred to as a charge-penetration energy. All of the attractive Coulomb interaction energy in Ar dimer is due to charge-penetration. Not surprisingly, errors in classical Coulomb interaction energies with respect to SAPT Coulomb interaction energies increase at shorter intermolecular distances where the quantum effects are larger.

Generally, all types of damping improve the classical treatment of Coulomb interactions relative to accurate quantum mechanics, but it is difficult to choose an approach that is the best for all dimers that are being considered here. For example, as seen in Figure 1, charge-charge damping and charge-charge plus higher-order exponential damping work equally well for Ar, methane, and CH₂Cl₂ dimers; the inclusion of higher-order damping is better (relative to SAPT) for ammonia and benzene sandwich dimers; using only charge-charge damping is better for methanol, HF, and benzene T-shaped dimers. The overlap-based damping performs better for H₂ and water dimers. Each type of damping has occasional failings. The overlap-based damping often underestimates the charge-penetration energy in weakly bound dimers whose interaction energies are typically dominated by dispersion forces (e.g. Ar, methane, benzene).

In summary, all types of damping functions provide a qualitative improvement in description of the Coulomb interaction energy relative to the corresponding quantum result obtained from the SAPT calculations.

5. Dispersion damping

Dispersion interactions govern much of the chemistry and physics in liquid and crystal phases and in many

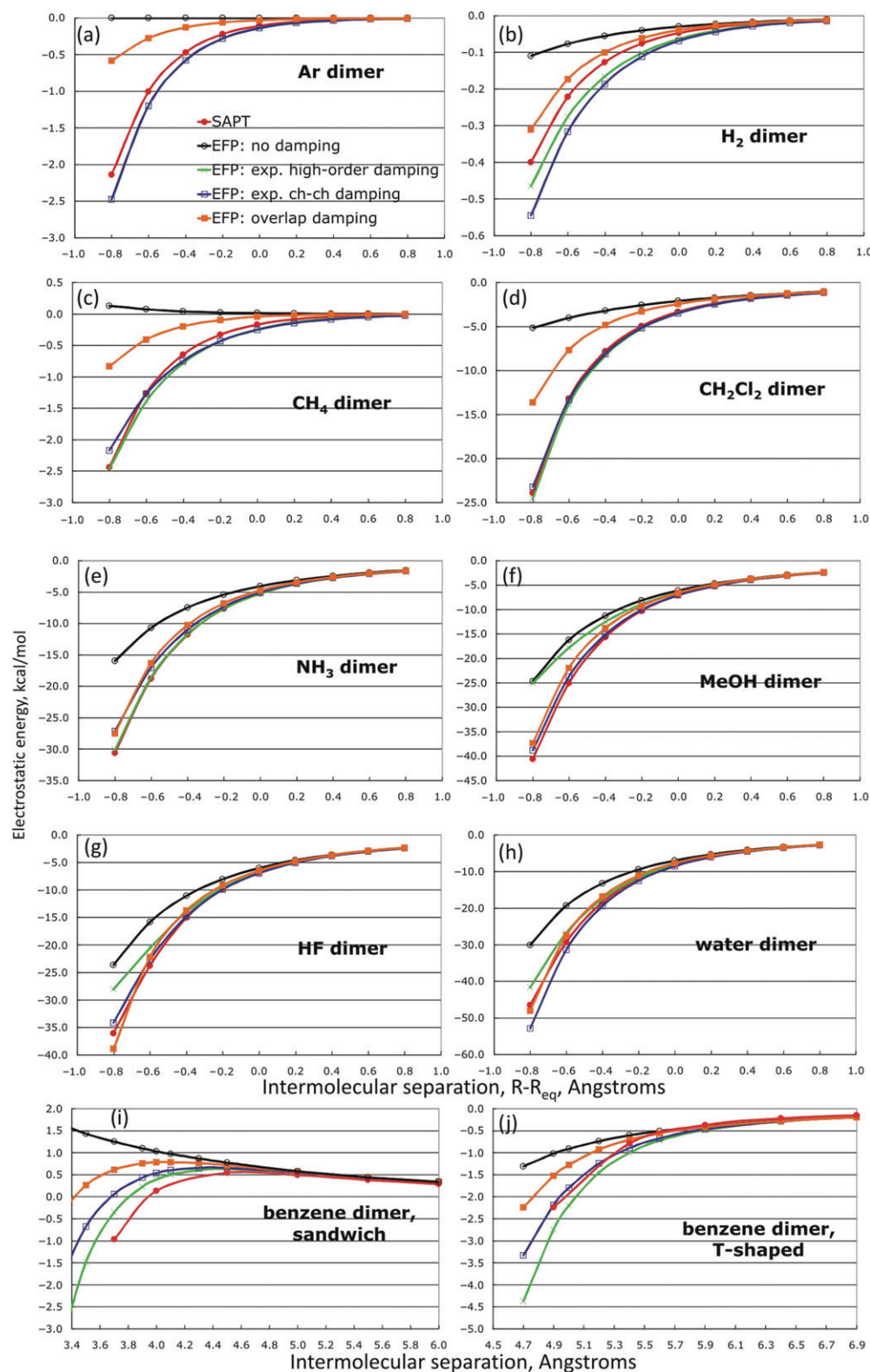


Figure 1. (Colour online) EFP electrostatic energies (kcal/mol) as a function of the intermolecular separation R (Å). ($R - R_{eq}$) values are plotted in graphs (a)–(h) (where R_{eq} is an equilibrium distance); the distances between the centres of masses of the monomers are plotted in graphs (i)–(j). The HF electrostatic energy from SAPT (red filled circles) and EFP electrostatic energies: without damping (black empty circles), with charge–charge exponential damping (blue empty squares), with exponential high-order damping (green crosses), and with overlap-based damping (orange filled circles) are shown.

biologically- and materials-relevant systems. In the spirit of other EFP terms, dispersion interactions in the EFP method are evaluated through a distributed approach, by using the dynamic polarizability tensors calculated at the localized molecular orbital (LMO) centroids⁶. Only the first (C_6/R^6) term is included in the expansion. Thus, the EFP dispersion energy is:

$$E_{disp} = \sum_{k \in A} \sum_{j \in B} \sum_{\alpha\beta\gamma\delta}^{x,y,z} T_{\alpha\beta}^{kj} T_{\gamma\delta}^{kj} \int_0^\infty dv \alpha_{\alpha\gamma}^k(iv) \alpha_{\beta\gamma}^j(iv) \quad (13)$$

where T are the electrostatic tensors of the second rank (see Appendix A) and α are the distributed dynamic polarizability tensors. k and j refer to LMO centroid points in A and B effective fragments, respectively. The integration in Equation (13) is performed by using a 12-point Gauss–Legendre quadrature. The dynamic polarizability tensors are obtained in the time-dependent Hartree–Fock procedure (TDHF). Only the isotropic part of the C_6 coefficients is used. In order to account for higher-order dispersion terms, the dispersion energies in EFP are scaled by 4/3 [6].

A great deal of theoretical work on optimizing functional forms and parameters for various force fields suggest that for accurate fitting to *ab initio* or experimental data, dispersion energies should be augmented by damping functions [35–42]. The Tang–Toennies formula [7] based on incomplete gamma functions seems to provide a reasonable description of dispersion damping:

$$f_{TT} = 1 - \exp(-\beta R) \sum_{n=1}^N \frac{(\beta R)^n}{n!} \quad (14)$$

where N is the order of the dispersion term (e.g. 6 for the R^{-6} term, 8 for the R^{-8} term), and β is the damping parameter. The optimal damping parameter β may be different for different species or different atomic centres; for example, some implementations suggest using the ionization energies to determine atomic damping parameters [43]. In the EFP implementation of dispersion, the damping parameter β was hard-coded to 1.5, based on a study of several small dimers at their equilibrium distances. Choosing a single value for β avoids introducing an empirically fitted parameter, but may not be appropriate for a broad range of species and a broad range of intermolecular distances. Therefore, an alternative approach is introduced here for damping dispersion energies in EFP. In this new approach information about intermolecular orbital overlap integrals (already available in the calculation of the intermolecular exchange repulsion) is used to define dispersion damping parameters.

5.1. Overlap-based formula for damping of dispersion

The formula for dispersion damping uses the fact that the distributed dynamic polarizability tensors used in the EFP method are determined at the LMO centroids. As shown by Equation (13), the total dispersion energy between a pair of EFPs is a sum of dispersion contributions between the pair of LMO centres of the two fragments. LMOs are also used in the calculation of the exchange-repulsion energies. This involves an on-the-fly computation of overlap and kinetic integrals between each pair of EFPs. For the dispersion interaction, the overlap integrals between pairs of LMOs are used to obtain damping parameters for the dispersion contributions due to the dynamic polarizability tensors centred at the corresponding pairs of LMOs. The formula for the overlap-based dispersion damping is in the spirit of the spherical Gaussian approximation used to determine the overlap-based Coulomb damping. That is, the overlap S between a pair of spherical Gaussian wave functions is:

$$S = \exp\left(-\frac{\alpha R^2}{2}\right). \quad (15)$$

The parameter α in Equation (15) is taken to be the damping parameter for dispersion. For mathematical simplicity, this is accomplished by modifying the Tang–Toennies damping formula (Equation 14) as follows:

$$f_S^n = 1 - \exp(-\alpha R^2) \sum_{n=1}^{N/2} \frac{(\alpha R^2)^n}{n!} = 1 - S^2 \sum_{n=1}^{N/2} \frac{(-2 \ln|S|)^n}{n!} \quad (16)$$

that is, the expansion is based on Gaussian rather than exponential functions. For consistency, the summation now goes up to $N/2$, where N is the power of the dispersion term. For $N=6$, Equation (16) can be rewritten as:

$$f_S^6 = 1 - S^2(1 - 2 \ln|S| + 2 \ln^2|S|), \quad (17)$$

where S is the overlap between LMOs centred at j and k . Thus, the final expression for the EFP dispersion energy between two EFPs A and B in this approach is:

$$E_{disp} = \sum_{k \in A} \sum_{j \in B} \frac{C_6(j, k) f_S^6(j, k)}{R_{jk}^6}. \quad (18)$$

Since the required overlap integrals are calculated for the exchange-repulsion term of EFP, there is no additional cost associated with this type of dispersion damping.

5.2. Computational results

Dispersion energy curves for the dimers are presented in Figure 2. For all of the dimers except the benzene dimer, both the dispersion and dispersion plus exchange-dispersion terms of SAPT are shown. The exchange-dispersion cross-term can be significant in hydrogen-bonded complexes like water or ammonia dimers, where it contributes about 15% of the dispersion energy at equilibrium and increases to ~25% at shorter distances. In its current implementation, EFP does not model the exchange-dispersion interaction. It is therefore important to compare the EFP dispersion interaction energies to the sum of the SAPT exchange-dispersion and dispersion terms, to ensure that the EFP dispersion term approximates their sum with reasonable accuracy.

Three different EFP curves are shown in Figure 2. These are the EFP dispersion energy without damping (green curve), the EFP dispersion energy with Tang-Toennies damping with damping parameter set to 1.5 for all species (blue curve), and the EFP dispersion energy with the overlap-based damping (orange curve). It is interesting that for the dimers whose interaction energies are dominated by dispersive forces (Ar, H₂, CH₄, benzene dimers), damping of the dispersion energies is not important. This is because the intermolecular distances in these dimers are relatively large, and quantum effects are relatively small. On the other hand, for hydrogen-bonded dimers, dispersion damping is necessary, since the EFP dispersion energies become too attractive at short separations. For all of the dimers considered here, the overlap-based damping works much better than the Tang-Toennies damping with a fixed parameter. The latter tends to ‘overdamp’ and produce dispersion interaction energies that are too weak. On the other hand, the overlap-based damping is much more sensitive than the Tang-Toennies damping to the nature of the interaction between molecules. For example, it adds only a minor correction to the dispersion energies in weakly bound clusters (e.g. H₂, Ar, methane dimers) but significantly modifies the strength of the dispersion interaction in hydrogen-bonded dimers, as it should. In general, the overlap-based damping provides a consistent improvement to the undamped EFP dispersion energies.

The EFP dispersion energies appear to be too weak in the hydrogen-bonded dimers, even taking into account the SAPT exchange-dispersion term. This may be due to the omission of the higher order dispersion contributions beyond R^{-6} (which could be underestimated even with the factor of 4/3 currently used in the EFP method for modeling these higher-order terms) and/or due to errors in the dynamic

polarizability tensors that are currently derived from time-dependent Hartree-Fock (TDHF). It has been suggested that time-dependent DFT (TDDFT) provides somewhat better accuracy for dynamic polarizabilities [44]. The implementation of TDDFT-based dynamic polarizabilities in EFP is in progress.

6. Polarization energy

Induction forces govern the structure and properties of water and other polarizable solvents, which unambiguously determine the chemistry of solutes. It is not surprising therefore that various attempts to incorporate induction or polarization interactions in force fields have been explored for about 30 years, with early works of Vesely [45], Stillinger and David [46], Stillinger [47], Barnes *et al.* [48], and Warshel [49]. Most polarizable models use isotropic, i.e. scalar polarizability points at atoms or molecular centres. Polarizabilities ascribed to molecules describe redistribution of the charge density within the molecule. In the EFP method, the polarization energy is modeled with asymmetric anisotropic polarizability tensors $\alpha_{\alpha\beta}$ located at the centroids of the localized molecular orbitals [2,3,50,51].

In the external field, the fragment A becomes polarized and develops induced dipoles located at polarizability points. These induced dipoles p^A are caused by the total field F_{total}^A , comprised of a static external field F^A and the field due to induced dipoles on the other fragments:

$$p_\gamma^A = \alpha_{\gamma\alpha}^A F_{\alpha,total}^A \quad (19)$$

$$F_{\alpha,total}^A = F_\alpha^A + F_{\alpha,ind}^A = F_\alpha^A + \sum_{B \neq A} T_{\alpha\beta}^{AB} p_\beta^B. \quad (20)$$

One can rewrite Equations (19) and (20) in the following form:

$$F_\alpha^A = (\alpha^A)_{\alpha\beta}^{-1} p_\beta^A - \sum_{B \neq A} T_{\alpha\beta}^{AB} p_\beta^B, \quad (21)$$

or

$$F_\alpha^A = \sum_{\beta B} D_{\alpha\beta}^{AB} p_\beta^B. \quad (22)$$

The last equation introduces tensor $D_{\alpha\beta}$; it is an operator that acts on dipoles to produce a field. The elements of $D_{\alpha\beta}$ are:

$$D_{\alpha\beta}^{AB} = \begin{cases} (\alpha^A)_{\alpha\beta}^{-1} & \text{if } A = B \\ 0 & \text{if } A \neq B \text{ in the same fragment} \\ -T_{\alpha\beta}^{AB} & \text{if } A \neq B \text{ in different fragments.} \end{cases} \quad (23)$$

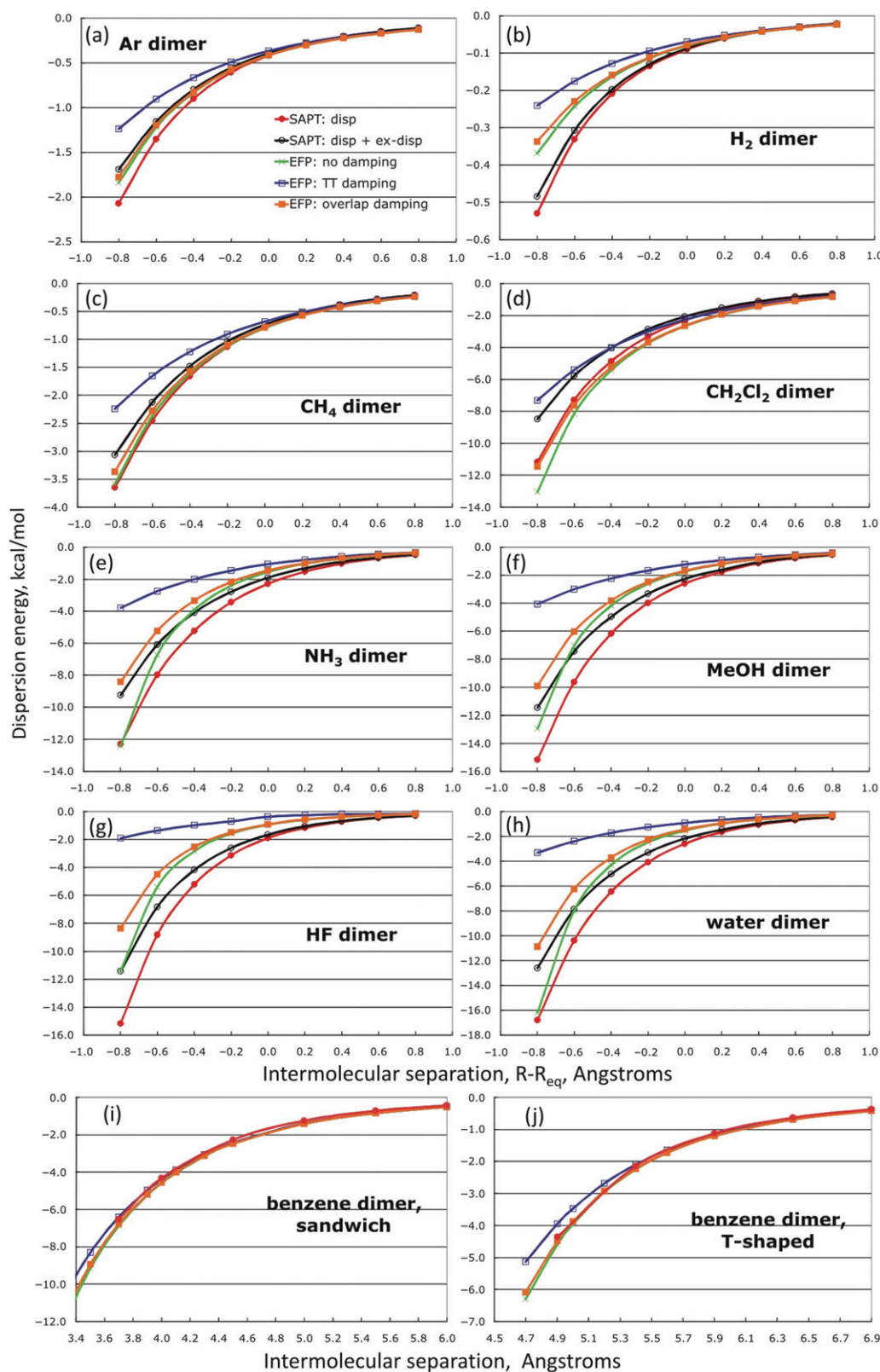


Figure 2. (Colour online) EFP dispersion energies (kcal/mol) as a function of the intermolecular separation R (Å) (see Figure 1 for notations). The SAPT energies: dispersion (red filled circles) and dispersion plus exchange-dispersion (black empty circles), and the EFP dispersion energies: without damping (green crosses), with Tang–Toennies damping with parameter $\beta = 1.5$ (blue empty squares), and with overlap-based damping (orange filled circles) are plotted.

The dimensions of the $D_{\alpha\beta}$ tensors are $(3N_{pol} \times 3N_{pol})$, where N_{pol} is the total number of polarizability points in all fragments; the factor 3 appears due to the three-component nature of the dipole vectors. The general form of $D_{\alpha\beta}$ is as follows:

$$D_{\alpha\beta}^{AB} = \begin{pmatrix} (\alpha^{I_1})_{\alpha\beta}^{-1} & \mathbf{0} & \mathbf{0} & -T_{\alpha\beta}^{J_1, I_1} & -T_{\alpha\beta}^{K_1, I_1} \\ \mathbf{0} & (\alpha^{I_2})_{\alpha\beta}^{-1} & \mathbf{0} & -T_{\alpha\beta}^{J_2, I_2} & -T_{\alpha\beta}^{K_2, I_2} \\ \mathbf{0} & \mathbf{0} & \dots & -T_{\alpha\beta}^{J_i, I_i} & -T_{\alpha\beta}^{K_i, I_i} \\ & -T_{\alpha\beta}^{I_1, J_1} & & (\alpha^{J_1})_{\alpha\beta}^{-1} & \mathbf{0} & \mathbf{0} \\ & \mathbf{0} & & (\alpha^{J_2})_{\alpha\beta}^{-1} & \mathbf{0} & -T_{\alpha\beta}^{K_2, J_2} \\ & \mathbf{0} & & \mathbf{0} & \mathbf{0} & \dots \\ & -T_{\alpha\beta}^{I_1, K_1} & & -T_{\alpha\beta}^{J_1, K_1} & (\alpha^{K_1})_{\alpha\beta}^{-1} & \mathbf{0} & \mathbf{0} \\ & & & & \mathbf{0} & (\alpha^{K_2})_{\alpha\beta}^{-1} & \mathbf{0} \\ & & & & \mathbf{0} & \mathbf{0} & \dots \end{pmatrix}, \quad (24)$$

where capital indexes I, J, K represent different fragments, and sub-indexes 1, 2, and i, j correspond to different polarizability points in each fragment. By introducing the inverse of $D_{\alpha\beta}$, one can further rewrite Equation (22) as follows:

$$p_{\alpha}^A = \sum_{\beta B} (D^{-1})_{\alpha\beta}^{AB} F_{\beta}^B. \quad (25)$$

Thus, in order to determine the induced dipoles in the system, one needs to find an inverse of matrix $D_{\alpha\beta}$. Alternatively, and more efficiently from the computational point of view, one can solve Equation (25) iteratively. The latter approach is used in the EFP method.

Once the induced dipoles p^A are found, one can obtain the polarization energy of the system as follows:

$$E_{ind} = \frac{1}{2} \sum_A p_{\alpha}^A F_{\alpha}^A. \quad (26)$$

The electrostatic operator of the second rank $T_{\alpha\beta}$, which appears in Equations (20), (21), (23) and (24), is proportional to $1/R^3$ (see Appendix A). At large separations between fragments, $T_{\alpha\beta}$ decays rapidly, the $D_{\alpha\beta}$ matrix becomes diagonally dominant, and the field of the induced dipole is determined by the polarizabilities. However, at shorter inter-fragment distances, $T_{\alpha\beta}$ tensors are larger and influence the dipole field. Finally, at very short separations, the matrix $D_{\alpha\beta}$ ceases to be positive definite, and, as a result, $(D^{-1})_{\alpha\beta}$ diverges. An explicit derivation of the limiting values R

at which $(D^{-1})_{\alpha\beta}$ diverges is given for the two-atom case in Ref. [9]. This condition is:

$$1 - (T_{\alpha\beta}^{AB})^2 \alpha_{\alpha\beta}^A \alpha_{\alpha\beta}^B = 0. \quad (27)$$

In terms of inter-centre distances, Equation (27) can be reformulated as:

$$R_{AB}^6 \propto \alpha_{\alpha\beta}^A \alpha_{\alpha\beta}^B. \quad (28)$$

The failure of the polarization model at short distances occurs because the classical multipole expansion fails in this region. This well-known problem [52] is often referred to as a ‘polarization collapse’. Even though the polarization collapse may occur only at short intermolecular separations, it still can be a troublesome issue if various regions of potential energy surface are investigated, as in molecular dynamics or Monte-Carlo simulations.

Two different approaches have been proposed to overcome this problem. One is to apply a damping function to suppress the singularity in the multipole interactions. To date, this has been investigated only for the dipole–dipole term [52–55]. Another, more fundamental, approach is to incorporate ‘charge-flow polarizabilities’, i.e. to allow charge redistribution within a molecule [56]. The latter procedure, however, is known to have poor convergence behaviour [56].

Two variants of polarization damping were explored within the EFP framework. In the first variant, damping functions for polarization have the same mathematical form as the exponential Coulomb damping functions. That is, the tensors in Equation (21), i.e. $T_{\alpha\beta}$ and F_{α} , are multiplied by the damping operators. This approach will be referred to as ‘exponential damping’. Especially important is damping of $T_{\alpha\beta}$, which results in a $1/R^0$ dependence, instead

of the original $1/R^3$ dependence of the $T_{\alpha\beta}$ operator and thus eliminates the divergence of $(D^{-1})_{\alpha\beta}$ (see Equation (24)). Thus, Equation (21) becomes:

$$\tilde{F}_\alpha^A = (\alpha^A)^{-1}_{\alpha\beta} p_\beta'^A - \sum_{B \neq A} \tilde{T}_{\alpha\beta}^{AB} p_\beta'^B \quad (29)$$

where

$$\tilde{F}_\alpha^A = q^B \tilde{T}_\alpha^{AB} + \mu_\beta^B \tilde{T}_{\alpha\beta}^{AB} + \Theta_{\beta\gamma}^B \tilde{T}_{\alpha\beta\gamma}^{AB} \quad (30)$$

is the damped field of the static multipoles. In this approach, the polarization energy of the system becomes:

$$E_{ind} = \frac{1}{2} \sum_A p_\alpha'^A \tilde{F}_\alpha^A \quad (31)$$

Note that in the last equation, the induced dipole (p_α') is also affected by damping functions, as follows from Equation (29).

As was discussed earlier, energy damping functions for each pair of multipole centres A and B $P^{AB}(\alpha, \beta)$ depend on two parameters, α and β . For electrostatic energies, these parameters are obtained from fitting the damped multipole potential to the quantum Hartree–Fock potential [5]. That is, each multipole expansion centre, i.e., each atom and bond mid-point, obtains a unique damping parameter α . If the distributed polarizability tensors were located at the multipole expansion points, it would be reasonable to use the same damping parameters for calculating polarization damping. However, in the EFP method, polarizability expansion points are centred at the LMO centroids; moreover, their total number is equal to the number of occupied orbitals, which may be different from the number of multipole centres. There is no straightforward way to determine the polarization damping parameters. Various choices of parameters for polarization damping are considered in the following subsection.

The second approach for damping polarization energies is similar in spirit to the Gaussian damping of dispersion energies. This approach will be referred to here as ‘Gaussian damping’. The same damping function f_{damp} is applied to all T and F_α tensors:

$$\begin{aligned} f_{damp}(\alpha, \beta, R) &= 1 - \exp(-\sqrt{\alpha\beta}R^2) (1 + \sqrt{\alpha\beta}R^2) \\ \tilde{T}_\alpha^{AB} &= f_{damp} T_\alpha^{AB} \\ \tilde{T}_{\alpha\beta}^{AB} &= f_{damp} T_{\alpha\beta}^{AB} \\ \tilde{T}_{\alpha\beta\gamma}^{AB} &= f_{damp} T_{\alpha\beta\gamma}^{AB} \\ \tilde{F}_\alpha^A &= f_{damp} F_\alpha^A. \end{aligned} \quad (32)$$

This damping function depends as R^4 in the vicinity of $R = 0$ and removes the singularity in all terms of the polarization energy. For each pair of interacting multipoles, two parameters (α and β) are needed. The choice of these parameters is discussed in the following subsection.

Implementation of the gradients of the polarization energy was discussed in detail in [51]. This derivation can be easily generalized to the case of modified (damped) electrostatic tensors and fields and is not discussed here.

6.1. Computational results

As discussed above, parameters for polarization damping functions cannot be determined *a priori*. Figure 3 shows the polarization energy curves for the water dimer obtained with exponential and gaussian-type damping schemes and with different values of polarization damping parameters. The parameters at all LMO centres and multipole centres were kept equal and varied simultaneously. The EFP polarization energy is compared with the HF part of SAPT induction energy (red curves) and a sum of HF SAPT induction and exchange-induction contributions. Correlation effects for induction energies are larger than they are for the Coulomb interactions and can account for up to 20% of the total polarization energy. For the sake of simplicity and straightforward comparison, the correlation contributions are not shown in Figure 3. SAPT induction and exchange-induction energies have large magnitudes and strongly cancel each other due to singularities in the electron-nuclear terms [14]. Therefore, as noted in [57], the sum of the SAPT induction and exchange-induction contributions approximates the pure induction energy defined as the interaction between occupied and virtual orbital subspaces on one fragment. This sum will be referred to as the ‘SAPT polarization energy’ in further discussion; the corresponding values are plotted with black curves in Figure 3. As expected, the EFP polarization energy overestimates the SAPT polarization energy, especially at shorter inter-fragment distances. The effect is opposite to that observed for Coulomb interactions. At $(R_0 - 1.0) \text{ \AA}$ the EFP polarization without damping diverges (aka ‘polarization collapse’). Both exponential and Gaussian damping improve the description of polarization energy. Optimal values of the damping parameters for water are 1.5–1.7 for exponential damping (Figure 3(a), (b)) and 0.6–0.8 for Gaussian damping (Figure 3(c), (d)). The exponential damping of polarization is used together with higher-order Coulomb damping; the

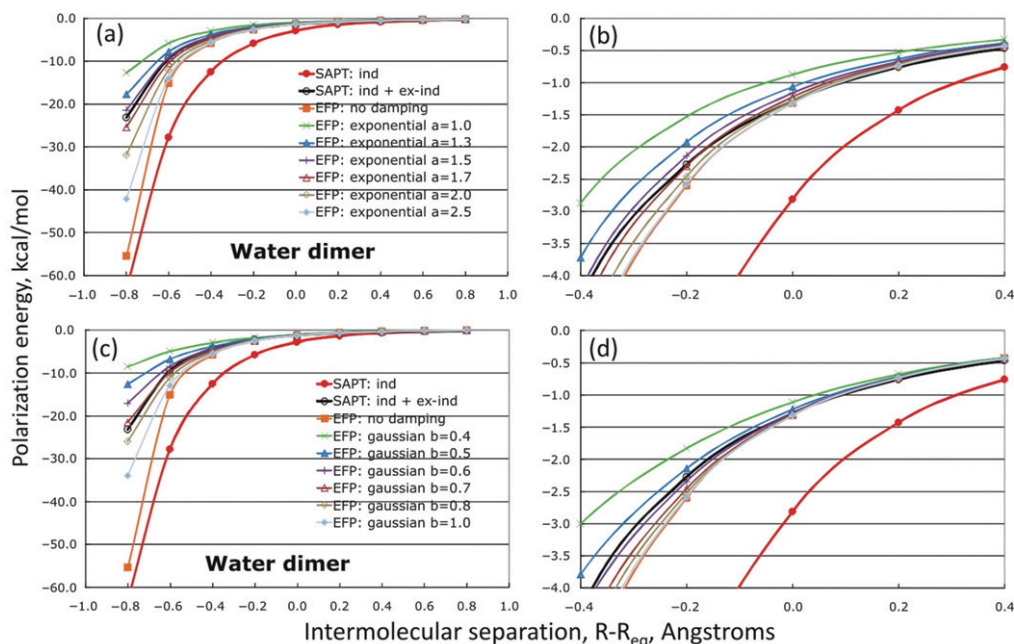


Figure 3. (Colour online) Damping of the induction energy (in kcal/mol) in the water dimer as a function of the intermolecular separation ($R - R_{eq}$) (Å), where R_{eq} is the equilibrium distance. (a–b): exponential damping of EFP induction with different values of damping parameter a . (c–d): Gaussian damping of induction with different values of damping parameter b . The SAPT energies: HF induction (red curves with filled circles) and HF induction plus exchange-induction (black curves with empty circles) are shown. Graphs (b) and (d) provide a larger view of the central region of graphs (a) and (c), respectively.

Coulomb damping parameters appear in the expressions of the polarization energy and the corresponding gradients. The observed optimal values of the polarization damping parameters for water are consistent with the typical values of Coulomb damping parameters found through fitting to the quantum electrostatic potentials. The suggested general strategy is to use the same values of damping parameters for all species. To ensure the stability of the EFP method at short inter-molecular separations, the values of 1.5 for exponential damping and 0.6 for Gaussian damping are chosen.

Figure 4 compares the EFP polarization energies with the SAPT polarization energies (i.e. a sum of induction and exchange-induction HF terms of SAPT) for the set of dimers considered here. The EFP polarization energies without polarization damping and with exponential damping with parameters set to 1.5 and Gaussian damping with parameters equal to 0.6 are shown. In general, the agreement between the EFP and SAPT polarization energies is not as good as the agreement between the EFP and SAPT Coulomb energies discussed above. The EFP formulation underestimates the polarization energy in Van der Waals bound complexes (Ar, H₂, CH₄ dimers). Due to the large intermolecular separations in these dimers,

damping does not play a significant role, except for the Ar dimer in which the classical polarization energy is zero. The polarization energy in hydrogen-bonded dimers is well described by EFP, and damping is very important in these complexes. In general, exponential damping works slightly better for these dimers. This might be due to either a better choice of the damping parameters or a favourable combination of the Coulomb and polarization damping parameters. On the other hand, Gaussian damping performs better in both configurations of the benzene dimer.

To summarize, both types of polarization damping functions with one *a priori* chosen parameter provide an improved agreement between the EFP and SAPT polarization energies. The exponential damping represents a general and physically meaningful approach for solving the problem of polarization collapse, since both electrostatic and polarization terms are treated analogously, i.e. both are damped with screening functions of the same form. Exponential damping seems to provide slightly better accuracy than Gaussian damping. However, the mathematical simplicity of Gaussian damping and its independence of the choice of Coulomb damping (for example, one could employ overlap-based or charge-charge damping for the Coulomb interactions) make it a reasonable choice.

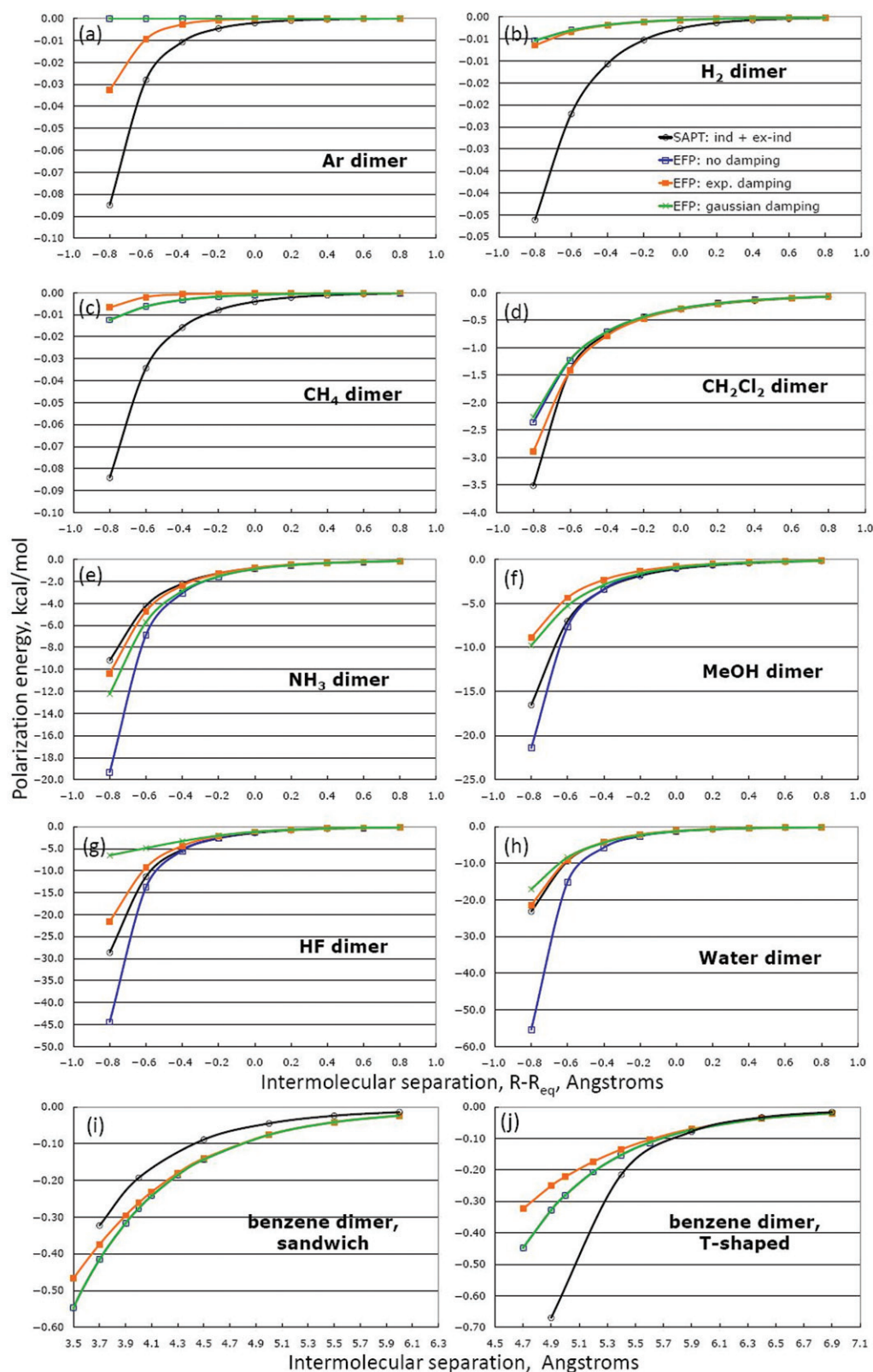


Figure 4. (Colour online) EFP polarization energies (kcal/mol) as a function of intermolecular separation R (Å) (see Figure 1 for notation). The HF SAPT induction plus exchange-induction energy (black empty circles) and the EFP polarization energies without damping (blue empty squares), with exponential damping with damping parameter $\alpha = 1.5$ (orange filled squares), with Gaussian damping with parameter $\beta = 0.6$ (green crosses) are plotted.

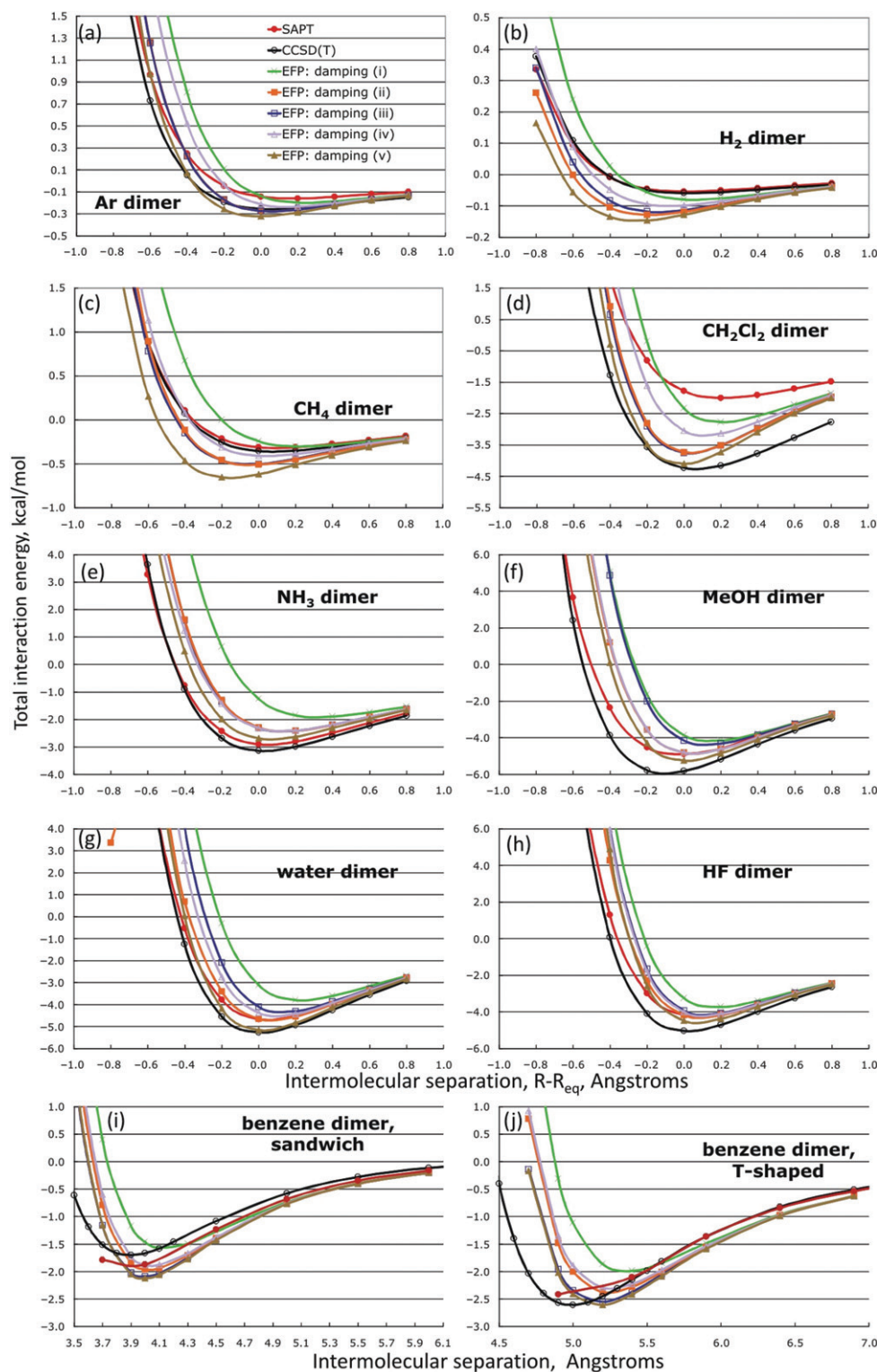


Figure 5. (Colour online) Total interaction energies in kcal/mol as a function of intermolecular separation R (Å) (see Figure 1 for notation). Total SAPT (red filled circles) and CCSD(T) interaction energies (black empty circles) are shown. The following total EFP energies are plotted: (i) EFP without electrostatic and induction damping and with TT dispersion damping (green crosses); (ii) EFP with exponential charge-charge damping, without induction damping and with TT dispersion damping (orange filled squares); (iii) EFP with exponential high-order electrostatic and induction dampings and with TT dispersion damping (blue empty squares); (iv) EFP with overlap-based electrostatic damping, Gaussian induction damping, and overlap-based dispersion damping (pink empty triangles); (v) EFP with exponential charge-charge electrostatic damping, Gaussian induction damping, and overlap-based dispersions damping (brown triangles).

7. Total interaction energies

Damping of the electrostatic, polarization, and dispersion terms is important for achieving correct asymptotic behavior and qualitative accuracy of the total EFP energies. Several different approaches for introducing damping have been suggested, with the accuracy of the alternative approaches being similar or only slightly different and system-dependent. This section considers the total EFP energies obtained with different sets of damping terms. A comparison of the total EFP, SAPT, and CCSD(T) interaction energies is shown in Figure 5. The following damping schemes are considered: (i) EFP Coulomb and polarization energies without damping, plus dispersion energy with Tang–Toennies damping (TT) with a 1.5 damping coefficient, (ii) Coulomb energy with charge–charge exponential damping, polarization energy without damping, dispersion energy with TT damping, (iii) charge–charge and higher-order exponential Coulomb damping, exponential polarization damping, and TT dispersion damping, (iv) Coulomb overlap-based damping, polarization Gaussian damping, and dispersion overlap-based damping, and (v) Coulomb charge–charge exponential damping, polarization Gaussian damping, and dispersion overlap-based damping. Scheme (i) is shown mainly as a reference; scheme (ii) has been the default for the general EFP method from 2005 to 2008.

First, note (Figure 5) that the SAPT and CCSD(T) potential energy curves do not always agree, probably due to incompleteness of the basis set and the basis set superposition error (BSSE) present in the CCSD(T) calculations. The CCSD(T) BSSE is especially obvious in the CH_2Cl_2 dimer, where the small 6-31+G* basis was used. However, some missing electron correlation in SAPT (compared to CCSD(T)) may be an additional reason for these disagreements. The EFP interaction energies are intrinsically free of the BSSE and therefore should better match the BSSE-free SAPT results. The SAPT interaction energy for the Ar dimer is too weak, and the CCSD(T) energy is much closer to the CCSD(T)/CBS limit of 0.27 kcal/mol.

The graphs in Figure 5 show that the EFP potential energy curves are often too repulsive at short distances. This is true even when the EFP equilibrium intermonomer separations are in a perfect agreement with the SAPT and CCSD(T) equilibrium distances (for example, in the water and HF dimers). There does not appear to be a single term in the EFP model that is responsible for this behaviour. Rather, a combination of slight discrepancies in several terms results in curves that are too repulsive. For example, in models (ii) and (iii), which include the TT dispersion damping, the underestimated dispersion at short distances is the main

origin of the curves that are too repulsive. On the other hand, the overly repulsive curves in model (iv) may occur due to underestimated Coulomb energies. Curves that are too repulsive may be partially due to the EFP exchange-repulsion contributions (not analyzed in this paper) that tend to be overly repulsive at short distances. The latter may be due to truncating the exchange-repulsion series in the intermolecular overlap at the quadratic S^2 term.

Not surprisingly, from all the considered models, model (i) (no damping in the electrostatic and induction terms) always provides the smallest interaction energies and longest equilibrium distances. Model (v), which combines the overlap-based dispersion damping, charge-charge electrostatic damping, and Gaussian induction damping, usually results in the largest binding energies and shortest separations. Models (ii)–(iv) are in between, and their performance is system-dependent. Model (iv) has better described (and usually larger) dispersion energies, while models (ii) and (iii) provide stronger Coulomb interactions.

In general, it is not easy to choose the model that generally provides the most consistent and accurate description of intermolecular binding. Model (i) is generally too repulsive, while model (ii) does not include polarization damping and can therefore result in a ‘polarization collapse’ at short separations (an example of this troublesome behavior can be seen in the water dimer graph, Figure 5(g)). Therefore, these two models can be eliminated from the list of possibilities. The three remaining models, (iii)–(v), all are reasonable. However, models (iv) and (v) are preferable, since they include the better description of dispersion. Model (v) generally results in more bound curves that overestimate the SAPT and CCSD(T) values in several cases. On average, model (iv) provides a balanced description of binding for most of the considered dimers. Therefore, the recommended approach is to use model (iv) as a default for all EFP calculations.

8. Conclusions

Intermolecular interactions play a major role in the chemistry of liquids, polymers, and biological systems. The analysis and accurate evaluation of these weak forces is challenging. The general effective fragment potential method has been developed as a tool for an accurate description of intermolecular interactions. However, in order to preserve the accuracy and applicability of the EFP at short intermolecular separations, and describe bonding in more strongly bound complexes, such as ionic salts, the long-range

interactions (Coulomb, induction, and dispersion) should be augmented by damping terms. These damping terms are supposed to mimic the strengthening of covalent interactions in the complex and provide the correct asymptotic behavior of the long-range classical forces in the short-range limit.

This paper presents an analysis of various damping functions for Coulomb, induction, and dispersion interactions. For this, the EFP interaction energy terms augmented by damping functions were compared with the SAPT energy terms at different intermolecular separations in ten weakly-bound dimers. The total binding energies of EFP were also compared with the CCSD(T) binding energies.

Three variants of electrostatic damping were considered: the exponential damping of the charge-charge interactions, the exponential damping of the charge-charge and higher multipolar interactions, and the damping derived from first principles, using the overlap of fragment LMOs in the spherical Gaussian approximation. All variants of damping improve the EFP electrostatic energies. The exponential damping generally performs better than the overlap-based damping. However, the first-principles-based overlap Coulomb damping may perform more consistently when different regions of a PES are considered. This topic will be investigated in more detail in a subsequent publication.

Damping of the polarization interactions is especially important because of the so called ‘polarization collapse’ which occurs when the self-consistent procedure for finding induced dipoles diverges at short separations. Exponential and Gaussian damping functions for induction interactions were developed and tested. Exponential damping functions are related to the higher order electrostatic damping functions; Gaussian damping is more similar to the damping functions used for dispersion. One parameter was introduced for each type of damping functions. Both kinds of damping improve the EFP induction energies and avoid the polarization collapse. The relative performance of these damping functions is system-dependent, with a slight preference for the exponential functions. However, analytical expressions for the Gaussian-like damping functions are much simpler; moreover, this damping is independent of the choice of Coulomb damping (exponential induction damping requires exponential higher order damping of the Coulomb interaction). Therefore, the Gaussian damping of the EFP induction is recommended.

The Tang-Toennies and overlap-based damping of dispersion interactions were investigated. The Tang-Toennies damping with a fixed damping coefficient

of 1.5 has previously been implemented in the EFP method. However, this damping significantly overdamps and results in dispersion interaction energies that are too weak, especially at short intermolecular separations. On the other hand, the overlap-based damping does not involve any damping parameter (the interfragment LMO overlap is used instead) and produces consistently good dispersion energies over the entire range of intermolecular separations. Therefore, the overlap-based damping function is recommended for the dispersion interactions in the EFP method.

The general conclusion, based on all of the foregoing discussions, is that one should use the scheme that employs overlap-based Coulomb and dispersion damping, and Gaussian induction damping in all future EFP applications. Employing this scheme results in a favorable comparison of the total EFP intermolecular energies with the SAPT and CCSD(T) energies. That is, in a set of ten dimers, EFP predicts intermolecular equilibrium distances (largest error is 0.2 Å) and binding energies (with absolute errors less than 0.5 kcal/mol). The consistently good performance of EFP is encouraging for further applications of the method to more complex molecular systems.

Acknowledgements

This work was supported by a SciDAC grant from the Department of Energy, administered by the Ames Laboratory.

References

- [1] P.N. Day, J.H. Jensen, M.S. Gordon, S.P. Webb, W.J. Stevens, M. Krauss, D. Garmer, H. Basch, and D. Cohen, *J. Chem. Phys.* **105**, 1968 (1996).
- [2] M.S. Gordon, L.V. Slipchenko, H. Li, and J.H. Jensen, *Ann. Rep. Comp. Chem.* **3**, 177 (2007).
- [3] M.S. Gordon, M.A. Freitag, P. Bandyopadhyay, J.H. Jensen, V. Kairys, and W.J. Stevens, *J. Phys. Chem. A* **105**, 293 (2001).
- [4] M.A. Freitag, M.S. Gordon, J.H. Jensen, and W.J. Stevens, *J. Chem. Phys.* **112**, 7300 (2000).
- [5] L.V. Slipchenko and M.S. Gordon, *J. Computat. Chem.* **28**, 276 (2007).
- [6] I. Adamovic and M.S. Gordon, *Mol. Phys.* **103**, 379 (2005).
- [7] K.T. Tang and J.P. Toennies, *J. Chem. Phys.* **80**, 3726 (1984).
- [8] B. Jeziorski, R. Moszynski, and K. Szalewicz, *Chem. Rev.* **94**, 1887 (1994).
- [9] A.J. Stone, *The Theory of Intermolecular Forces* (Oxford University Press, Oxford, 1996).

- [10] J.H. Jenson and M.S. Gordon, *Mol. Phys.* **89**, 1313 (1996).
- [11] W.J. Hehre, R. Ditchfield, and J.A. Pople, *J. Chem. Phys.* **56**, 2257 (1972).
- [12] R.D. Amos, N.C. Handy, P.J. Knowles, J.E. Rice, and A.J. Stone, *J. Phys. Chem.* **89**, 2186 (1985).
- [13] H. Li, M.S. Gordon, and J.H. Jensen, *J. Chem. Phys.* **124**, 214108 (2006).
- [14] K. Patkowski, B. Jeziorski, and K. Szalewicz, *J. Mol. Struct.-Theochem.* **547**, 293 (2001).
- [15] I. Adamovic and M.S. Gordon, *J. Phys. Chem. A* **110**, 10267 (2006).
- [16] I. Adamovic, H. Li, M.H. Lamm, and M.S. Gordon, *J. Phys. Chem. A* **110**, 519 (2006).
- [17] Smith, T., Slipchenko, L.V., Gordon, M.S. *J. Phys. Chem.* **112**, 5286 (2008).
- [18] M.W. Schmidt, K.K. Baldridge, J.A. Boatz, S.T. Elbert, M.S. Gordon, J.H. Jensen, S. Koseki, N. Matsunaga, K.A. Nguyen, S.J. Su, T.L. Windus, M. Dupuis, and J.A. Montgomery, *J. Computat. Chem.* **14**, 1347 (1993).
- [19] M.S. Gordon and M.W. Schmidt, in *Theory and Applications of Computational Chemistry*, edited by C.E. Dykstra, G. Frenking, K.S. Kim, and G.E. Scuseria (Elsevier, Amsterdam, 2005).
- [20] K.A. Peterson and T.H. Dunning, *J. Chem. Phys.* **102**, 2032 (1995).
- [21] K. Raghavachari, G.W. Trucks, and J.A. Pople, Head-Gordon, M. *Chem. Phys. Lett.* **157**, 479 (1989).
- [22] T.H. Dunning, *J. Chem. Phys.* **90**, 1007 (1989).
- [23] R.A. Kendall, T.H. Dunning, and R.J. Harrison, *J. Chem. Phys.* **96**, 6796 (1992).
- [24] D.E. Woon, *J. Chem. Phys.* **100**, 2838 (1994).
- [25] C. Moller and S. Plesset, *Phys. Rev.* **46**, 618 (1934).
- [26] T. Clark, J. Chandrasekhar, G.W. Spitznagel, and P.V. Schleyer, *J. Computat. Chem.* **4**, 294 (1983).
- [27] M.J. Frisch, J.A. Pople, and J.S. Binkley, *J. Chem. Phys.* **80**, 3265 (1984).
- [28] R. Krishnan, J.S. Binkley, R. Seeger, and J.A. Pople, *J. Chem. Phys.* **72**, 650 (1980).
- [29] M.O. Sinnokrot, E.F. Valeev, and C.D. Sherrill, *J. Am. Chem. Soc.* **124**, 10887 (2002).
- [30] M.M. Francl, W.J. Pietro, W.J. Hehre, J.S. Binkley, M.S. Gordon, D.J. Defrees, and J.A. Pople, *J. Chem. Phys.* **77**, 3654 (1982).
- [31] P.C. Hariharan and J.A. Pople, *Theoretica Chimica Acta* **28**, 213 (1973).
- [32] M.O. Sinnokrot and C.D. Sherrill, *J. Phys. Chem. A* **108**, 10200 (2004).
- [33] V. Kairys and J.H. Jensen, *Chem. Phys. Lett.* **315**, 140 (1999).
- [34] J.H. Jensen, *J. Chem. Phys.* **104**, 7795 (1996).
- [35] J.T. Ajit, *J. Chem. Phys.* **89**, 2092 (1988).
- [36] D. Cvetko, A. Lausi, A. Morgante, F. Tommasini, P. Cortona, and M.G. Dondi, *J. Chem. Phys.* **100**, 2052 (1994).
- [37] A.G. Donchev, *Phys. Rev. B* **74**, 235401 (2006).
- [38] G. Ihm, W.C. Milton, T. Flavio, and G. Scoles, *J. Chem. Phys.* **87**, 3995 (1987).
- [39] S.H. Patil, K.T. Tang, and J.P. Toennies, *J. Chem. Phys.* **116**, 8118 (2002).
- [40] M. Wilson, P.A. Madden, N.C. Pyper, and J.H. Harding, *J. Chem. Phys.* **104**, 8068 (1996).
- [41] A.J. Stone and A.J. Misquitta, *Int. Rev. Phys. Chem.* **26**, 193 (2007).
- [42] R.J. Wheatley and W. Meath, *J. Mol. Phys.* **80**, 25 (1993).
- [43] K.T. Tang, J.P. Toennies, and C.L. Yiu, *Phys. Rev. Lett.* **74**, 1546 (1995).
- [44] S. Hirata, S. Ivanov, R.J. Bartlett, and I. Grabowski, *Phys. Rev. A* **71**, 032507 (2005).
- [45] F.J. Vesely, *J. Computat. Phys.* **24**, 361 (1977).
- [46] F.H. Stillinger and C.W. David, *J. Chem. Phys.* **69**, 1473 (1978).
- [47] F.H. Stillinger, *J. Chem. Phys.* **71**, 1647 (1979).
- [48] P. Barnes, J.L. Finney, J.D. Nicholas, and J.E. Quinn, *Nature* **282**, 459 (1979).
- [49] A. Warshel, *J. Phys. Chem.* **83**, 1640 (1979).
- [50] J.H. Jensen, P.N. Day, M.S. Gordon, H. Basch, D. Cohen, D.R. Garmer, M. Kraus, and W.J. Stevens, *Modeling Hydrogen Bond* **569**, 139 (1994).
- [51] H. Li, H.M. Netzloff, and M.S. Gordon, *J. Chem. Phys.* **125**, 194103 (2006).
- [52] B.T. Thole, *Chem. Phys.* **59**, 341 (1981).
- [53] M. Masia, M. Probst, and R. Rey, *Chem. Phys. Lett.* **420**, 267 (2006).
- [54] J.P. Piquemal, L. Perera, G.A. Cisneros, P.Y. Ren, L.G. Pedersen, and T.A. Darden, *J. Chem. Phys.* **125**, 054511 (2006).
- [55] K.J. Miller, *J. Am. Chem. Soc.* **112**, 8543 (1990).
- [56] C.R. Lesueur and A.J. Stone, *Mol. Phys.* **78**, 1267 (1993).
- [57] A.J. Misquitta and A.J. Stone, *J. Chem. Theory Computat.* **4**, 7 (2008).

Appendix A

$$T = \frac{1}{4\pi\epsilon_0 R}. \quad (\text{A1})$$

$$T_\alpha = -\frac{R_\alpha}{4\pi\epsilon_0 R^3}. \quad (\text{A2})$$

$$T_{\alpha\beta} = \frac{3R_\alpha R_\beta - R^2 \delta_{\alpha\beta}}{4\pi\epsilon_0 R^5}. \quad (\text{A3})$$

$$T_{\alpha\beta\gamma} = -\frac{15R_\alpha R_\beta R_\gamma - 3R^2(R_\alpha \delta_{\beta\gamma} + R_\beta \delta_{\alpha\gamma} + R_\gamma \delta_{\alpha\beta})}{4\pi\epsilon_0 R^7}. \quad (\text{A4})$$

$$D_{\alpha\beta} = R_\alpha R_\beta. \quad (\text{A5})$$

$$f_1 = -\exp(-\alpha R)(1 + \alpha R). \quad (\text{A6})$$

$$f_2 = -\exp(-\alpha R)\frac{\alpha^2}{R^3}. \quad (\text{A7})$$

Appendix B

$$\begin{aligned}
P_0(\alpha, \beta, R) &= -\exp(-\alpha R) \frac{\beta^2}{\beta^2 - \alpha^2} \\
&\quad - \exp(-\beta R) \frac{\alpha^2}{\alpha^2 - \beta^2} \\
P_0(\alpha, \beta, R)_{\beta \rightarrow \infty} &= -\exp(-\alpha R) \\
P_0(\alpha, \beta, R)_{\beta=\alpha} &= -\exp(-\alpha R)(1 + \alpha R) \\
P_0(\alpha, \beta, R)_{\beta \rightarrow \infty, R \rightarrow 0} &= -1 + \frac{1}{2}(\alpha R)^2 \\
P_0(\alpha, \beta, R)_{\beta=\alpha, R \rightarrow 0} &= -1 + \frac{1}{6}(\alpha R)^3. \tag{B1}
\end{aligned}$$

$$\begin{aligned}
P_1(\alpha, \beta, R) &= -\exp(-\alpha R) \frac{\beta^2}{\beta^2 - \alpha^2} (1 + \alpha R) \\
&\quad - \exp(-\beta R) \frac{\alpha^2}{\alpha^2 - \beta^2} (1 + \beta R) \\
P_1(\alpha, \beta, R)_{\beta \rightarrow \infty} &= -\exp(-\alpha R)(1 + \alpha R) \\
P_1(\alpha, \beta, R)_{\beta=\alpha} &= -\exp(-\alpha R) \left(1 + \alpha R + \frac{1}{2}(\alpha R)^2 \right) \\
P_1(\alpha, \beta, R)_{\beta \rightarrow \infty, R \rightarrow 0} &= -1 + \frac{1}{2}(\alpha R)^2 \\
P_1(\alpha, \beta, R)_{\beta=\alpha, R \rightarrow 0} &= -1 + \frac{1}{6}(\alpha R)^3. \tag{B2}
\end{aligned}$$

$$\begin{aligned}
P_2(\alpha, \beta, R) &= -\exp(-\alpha R) \frac{\beta^2}{\beta^2 - \alpha^2} \frac{\alpha^2}{R^3} \\
&\quad - \exp(-\beta R) \frac{\alpha^2}{\alpha^2 - \beta^2} \frac{\beta^2}{R^3} \\
P_2(\alpha, \beta, R)_{\beta \rightarrow \infty} &= -\exp(-\alpha R) \frac{\alpha^2}{R^3} \\
P_2(\alpha, \beta, R)_{\beta=\alpha} &= -\exp(-\alpha R) \frac{\alpha^3}{2R^2} \\
P_2(\alpha, \beta, R)_{\beta \rightarrow \infty, R \rightarrow 0} &= -\frac{\alpha^2}{R^3} \\
P_2(\alpha, \beta, R)_{\beta=\alpha, R \rightarrow 0} &= -\frac{\alpha^3}{2R^2}. \tag{B3}
\end{aligned}$$

$$\begin{aligned}
P_3(\alpha, \beta, R) &= \exp(-\alpha R) \frac{\beta^2}{\beta^2 - \alpha^2} \frac{\alpha^2(\alpha R + 3)}{R^5} \\
&\quad + \exp(-\beta R) \frac{\alpha^2}{\alpha^2 - \beta^2} \frac{\beta^2(\beta R + 3)}{R^5} \\
P_3(\alpha, \beta, R)_{\beta \rightarrow \infty} &= \exp(-\alpha R) \frac{\alpha^2(\alpha R + 3)}{R^5} \\
P_3(\alpha, \beta, R)_{\beta=\alpha} &= \exp(-\alpha R) \frac{\alpha^3(1 + 0.5\alpha R)}{R^4}. \tag{B4}
\end{aligned}$$

$$\begin{aligned}
P_4(\alpha, \beta, R) &= \exp(-\alpha R) \frac{\beta^2}{\beta^2 - \alpha^2} \alpha^2 \\
&\quad + \exp(-\beta R) \frac{\alpha^2}{\alpha^2 - \beta^2} \beta^2 \\
P_4(\alpha, \beta, R)_{\alpha \rightarrow \infty} &= \exp(-\beta R) \beta^2 \\
P_4(\alpha, \beta, R)_{\beta=\alpha} &= \exp(-\alpha R) (\alpha R) \alpha^2. \tag{B5}
\end{aligned}$$